JGR Atmospheres

RESEARCH ARTICLE
10.1029/2025JD045561

Trace Elements in Arctic Ocean Aerosols: Contemporary Status and Decadal Variability

Wenkai Guan[1], Musheng Lan[2], Ying Ping Lee[3], Yulong Huang[1], Hui Lin[2], Mengli Chen[4], Jianfang Chen[5], and Ruifeng Zhang[1,2]

[1]School of Oceanography, Shanghai Jiao Tong University, Shanghai, China, [2]Polar Research Institute of China, Shanghai, China, [3]Independent Researcher, Kuala Lumpur, Malaysia, [4]Tropical Marine Science Institute, National University of Singapore, Singapore, Singapore, [5]Key Laboratory of Marine Ecosystem Dynamics, Second Institute of Oceanography, Ministry of Natural Resources, Hangzhou, China

Key Points:

- The Arctic Ocean exhibits globally low levels of both trace element concentrations and the enrichment of these anthropogenic trace elements
- Sea ice/snow resuspension causes comparable or higher mineral trace element fluxes in the central Arctic than in the peripheral Arctic
- Arctic shipping intensification caused near-doubling of V concentrations and enrichment degree

Supporting Information:

Supporting Information may be found in the online version of this article.

Correspondence to:

R. Zhang,
ruifengzhang@sjtu.edu.cn

Citation:

Guan, W., Lan, M., Lee, Y. P., Huang, Y., Lin, H., Chen, M., et al. (2026). Trace elements in Arctic Ocean aerosols: Contemporary status and decadal variability. *Journal of Geophysical Research: Atmospheres*, *131*, e2025JD045561. https://doi.org/10.1029/2025JD045561

Received 2 OCT 2025
Accepted 4 JAN 2026

Author Contributions:

Conceptualization: Wenkai Guan, Musheng Lan, Ying Ping Lee, Hui Lin, Mengli Chen, Jianfang Chen, Ruifeng Zhang
Data curation: Wenkai Guan, Ruifeng Zhang
Formal analysis: Wenkai Guan, Musheng Lan, Ying Ping Lee, Hui Lin, Mengli Chen, Jianfang Chen
Funding acquisition: Hui Lin, Ruifeng Zhang
Investigation: Wenkai Guan, Musheng Lan, Mengli Chen, Jianfang Chen
Methodology: Wenkai Guan, Musheng Lan, Hui Lin, Mengli Chen, Jianfang Chen
Supervision: Ruifeng Zhang
Validation: Wenkai Guan
Visualization: Wenkai Guan, Yulong Huang
Writing – original draft: Wenkai Guan

Abstract Aerosol trace element (TE) transport serves as a critical driver of marine TE biogeochemical cycles and climate feedback systems. In the rapidly warming Arctic Ocean (AO), however, the contemporary distribution patterns and decadal variability of aerosol TE deposition remain poorly constrained, representing a critical gap in our understanding of current and future Arctic environmental changes. Here, we present extensive shipboard observations of 13 aerosol TEs across the AO during summer 2024. TE concentrations and the enrichment levels of these anthropogenic TEs rank among the lowest globally observed in the AO. The comparable or even elevated mineral- dominated TE concentrations and deposition fluxes (Al, Fe) in the Central AO than Peripheral AO challenge current dust models, potential influenced by sea ice/snow resuspension. Coal combustion (As, Se), non-exhaust vehicular emissions (Ni, Cr), and metallurgical activities (Zn) emerged as primary anthropogenic sources, with detectable anthropogenic imprint even in mineral-dominated TEs (e.g., Fe, Mn). Decadal comparisons with historical records revealed a near ten-fold reduction in Pb and Cd enrichment, contrasting with a near-doubling of V enrichment driven by intensified Arctic shipping. Moreover, the distinct aerosol Fe/Al fractionation between this study and historical observations likely arises from mixing inputs of anthropogenic Fe-rich particles and permafrost-derived Fe-depleted weathering products, which amplify uncertainties in Fe flux estimations derived from dust proxy approaches. This study provides advance understanding of aerosol TE dynamics in the warming Arctic and provide critical constraints for polar biogeochemical cycles.

Plain Language Summary The delivery of aerosol trace elements (TEs) constitutes a critical climate feedback mechanism. The AO serves as a harbinger of climate change, where rapid transformations, including declining sea ice cover, thawing permafrost, and intensifying shipping activities are converging to exert multifaceted pressures on source-sink processes of aerosol TEs. Despite this urgency, significant observational gaps persist regarding their current state and decadal changes. This study leveraged comprehensive ship-based observations traversing the AO and characterized the spatial distribution, enrichment mechanisms, and deposition fluxes of aerosol TEs. Our findings reveal that the Arctic exhibits among the lowest TE deposition fluxes documented globally for open oceans, alongside minimal enrichment levels of these anthropogenic TEs. We emphasize that particle resuspension from sea ice surfaces, a previously overlooked process, is identified as a key driver of elevated TE concentrations in the Central AO. Decadal-scale trends further demonstrate a near tenfold reduction in Pb and Cd enrichment, reflecting diminished anthropogenic influences across the Arctic, while a near doubling of V enrichment directly correlates with expanding shipping activity. Critically, Fe cycling manifests unique complexity due to mixed influences from anthropogenic sources and local weathering products. These insights substantially advance our capacity to reconstruct historical and project future Arctic climate trajectories.

1. Introduction

Aerosol transport is vital for Earth's climate and environment because it delivers bio-essential trace elements (TEs) to the oceans (Jickells et al., 2005). This process helps alleviate micronutrient limitations in seawater, enhances primary productivity, and facilitates carbon sequestration through the biological pump (Ducklow et al., 2001; Weis et al., 2024). Additionally, while certain trace elements (e.g., Cu, As) exhibit bioaccumulative toxicity and adversely affect marine biota at supra-threshold concentrations (Duan et al., 2025; Paytan

Writing – review & editing:
Wenkai Guan, Ruifeng Zhang

et al., 2009), some TEs (e.g., Al, Mn, Cd) serve as valuable tracers for marine material sources and internal geochemical processes (Zhang et al., 2019; Zheng et al., 2019). However, the accurate assessment of aerosol deposition remains challenging due to the scarcity of observational data, particularly in the remote marine and polar regions (Mahowald et al., 2018; Schmale et al., 2021). The Arctic Ocean (AO) serves as an intermediary between the Pacific and Atlantic Oceans, playing a pivotal role in the global TE biogeochemical cycling (Krisch et al., 2022; Whitmore et al., 2025). Over the past 50 years, the Arctic has experienced warming rates more than twice the global average, resulting in reduced sea ice expand, increased weathering, and accelerated permafrost thawing (Masson-Delmotte et al., 2021; Rantanen et al., 2022). These changes further significantly affect aerosol TE emissions and their transport into the AO (Heintzenberg et al., 2015; Pernov et al., 2022; Willis et al., 2018). Therefore, monitoring aerosol TEs in the Arctic is crucial for understanding the evolving dynamics of global biogeochemistry in the context of ongoing climate change.

Nitrogen (N) has been definitively recognized as the key limiting nutrient for biological productivity in the AO (Browning & Moore, 2023) rather than bioavailable TEs (Fe, Zn, Mn, Cd, etc.), as the broadly sufficient supply of bioavailable TEs derived from continental shelves and fluvial sources (Kanna et al., 2025; Whitmore et al., 2025; Zhang et al., 2019, 2021). Nevertheless, stoichiometrically induced TE limitations have been increasingly documented in specific AO regions or during certain periods (Klunder et al., 2012; Zhang et al., 2021). A representative study in the eastern AO demonstrated that constrained Fe bioavailability in subsurface layers may reduce phytoplankton nitrogen uptake efficiency by nearly 50% (Rijkenberg et al., 2018). Aerosol deposition represents an additional significant source of bioavailable TEs in the AO, supplementing inputs from continental shelves and rivers. Illustratively, De Vera et al. (2021) quantified that annual aerosol-derived bioavailable Fe fluxes are comparable in magnitude to those from the Mackenzie River—the principal fluvial source to the Canada Basin. Against the backdrop of accelerated Arctic warming and permafrost degradation, mineral dust emissions from circum-Arctic regions are emerging as a growing dust source (Gao et al., 2019), highlighting the increasing importance of aerosol-mediated delivery of bioavailable TEs to the Arctic marine system.

The long-range transport of anthropogenic air masses has emerged as a significant source of aerosol TEs in the AO (Heintzenberg et al., 2015; Ji et al., 2019; Lannefors et al., 1983; Xie et al., 2006), which even contributes to Arctic haze formation (Shaw, 1995; Zhan et al., 2014). Zhan et al. (2017) reported anthropogenic influence on the alterations in the physicochemical properties of aerosols at Ny-Ålesund, while Marsay, Kadko, et al. (2018) noted significant enrichments of Ni, Cu, Zn, Pb, and Cd in aerosols from the western AO. Furthermore, Pb isotopes have traced the influence of industrial emissions to the Canadian Arctic from Russia, Europe, and China (De Vera et al., 2021). Besides, as human activities such as shipping, and oil extraction continue to expand in the Arctic region, regional emissions are projected to increase (Willis et al., 2018). For instance, Zhan et al. (2014) found that ship activity tripled aerosol mass and significantly elevated concentrations of V and Ni at Ny-Ålesund, underscoring the importance of elucidating Arctic aerosol TE enrichment levels, sources, and their contribution to AO TE supply. However, much of the existing data is derived from land-based stations along the Arctic periphery, leaving a notable scarcity of ship-based observations utilizing clean sampling techniques, particularly in the central Arctic basin, which has resulted in critical gaps in aerosol multi-TE records (Kadko et al., 2016; Maenhaut et al., 1996; Marsay, Kadko, et al., 2018; Xie et al., 2006). With ongoing Arctic warming, the biogeochemical cycling of TEs is rapidly changing (He et al., 2025; Tovar-Sánchez et al., 2010; Whitmore et al., 2025). As sea ice retreats, aerosol TEs are more likely to deposit directly into surface waters, bypassing the processing typically associated with sea ice (Confer et al., 2023; Marsay, Kadko, et al., 2018; Stephens et al., 2024), whereas the expansion of freshwater coverage may alter deposition patterns due to increased summer fog (Danielson et al., 2020; Zhao et al., 2022). Therefore, investigating aerosol TE enrichment and fluxes over the AO is essential for improving current data sets and deepening our understanding of this rapidly evolving environment.

This study aims to (a) characterize the spatial distribution of various aerosol TEs, (b) assess their enrichment levels and identify the primary sources, and (c) estimate their deposition fluxes in the AO. By addressing these objectives, this research offers an aerosol-based perspective on the dynamics of TEs in the rapidly changing Arctic environment. To achieve these goals, an aerosol sampling campaign was conducted during the 14th Chinese National Arctic Research Expedition (CHINARE). This data set will help fill a critical observational gap in AO and enhance understanding of the distribution, sources, and biogeochemical significance of aerosol TEs under ongoing climate change.

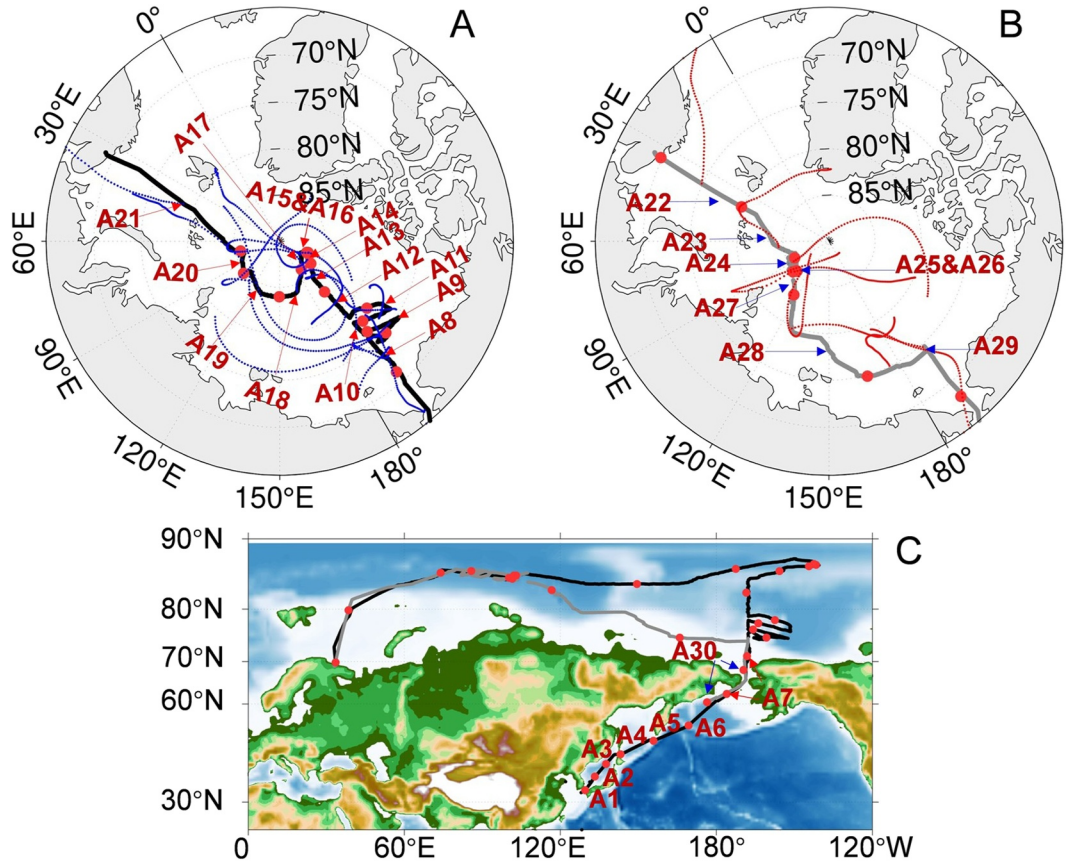

Figure 1. Cruise track and Sampling station information. Panel (a) shows the black solid line representing the outbound cruise track from the Bering Strait to Murmansk, Russia, through the Arctic Ocean region, while Panel (b) displays the gray solid line denoting the return cruise track from Murmansk, Russia, to the Bering Strait through the Arctic Ocean region. Panel (c) illustrates sampling information from the Northwest Pacific marginal sea during the sampling period. Red dots indicate the start or end positions of samples, with solid lines connecting two red dots representing the sampling tracks of individual aerosol samples, and numbered IDs corresponding to sample identifiers. Additionally, the blue dashed line in Panel (a) and the red dashed line in Panel (b) display the 3-day air mass backward trajectories of samples during the sampling period. Additionally, in panel (c), the black line depicts the outbound trajectory to the Arctic Ocean, while the gray line shows the return path; arrows link sample labels to their respective track segments, with red signifying outbound samples and blue representing return samples.

2. Materials and Methods

2.1. Filter Preparation and Sample Collection

Aerosol samples were collected using Whatman 41 cellulose filters (203 mm × 254 mm, PN 1441-866) that underwent rigorous acid-cleaning to minimize TE contaminations. The cleaning procedure was conducted in a Class-100 laminar flow bench, as detailed by Ge et al. (2024). In brief, the filters were soaked three times in freshly prepared 3 M HCl (trace metal grade, Fisher) for 5 days during each cycle. This was followed by three 24-hr soaks in 0.5 M HCl (distilled from trace metal grade), with thorough rinsing in ultrapure water (18.2 MΩ·cm) to achieve a neutral pH after each step. The cleaned filters were then air-dried in the class-100 laminar flow bench and stored in double-sealed polyethylene bags until further use.

During the 14th CHINARE cruise, 30 aerosol samples were collected near an 80-day cruise aboard the Chinese icebreaker *R/V XueLong 2* from 7 July to 24 September 2024 (Figure 1 and Table S1 in Supporting Information S1). The sampling employed a high-volume total suspended particulate (TSP) sampler (TE-5170DX, Tisch) that operated at a constant flow rate of ∼1.13 m^3 min^{-1}. To minimize contamination from ship exhaust and sea spray, the sampler was mounted on the forward railing of the compass deck, ∼18 m above sea level. Sampling was automatically regulated by a controller equipped with a Vaisala WXT530 wind sensor, activating only when the

relative wind direction was within ±60° of the vessel's heading and the wind speed exceeded 2 m s^{-1} for a period of over 300 s. Following collection, the filters were folded, sealed in clean polyethylene bags, and stored at −20°C in a contaminant-free refrigerator.

2.2. Elemental Concentration Determination

Following the edge-trimming process, the membrane, which had been folded after sampling, was divided into 16 equal sections on a Teflon plate using a ceramic knife. Each section represented 5.6% of the effective sampling area. Two symmetrically positioned sections were subsequently transferred to a pre-cleaned 7 mL polyfluoroalkoxy vial and subjected to acid digestion using 4 mL of a mixed acid composed of 12 M HNO_3 (distilled from trace metal grade) and 6 M HF (Fisher, Optima grade). The sealed vial was gradually heated on a hot plate to 160°C until complete digestion was achieved. The digestate was then evaporated to near dryness, followed by the addition of 0.5 mL of 15 M HNO_3, with subsequent re-evaporation. This step was repeated once to ensure complete removal of residual HF. Finally, the residue was redissolved in 10 mL of 1 M HNO_3 and transferred to a trace metal clean centrifuge tube for elemental analysis. The concentrations of TE were measured by inductively coupled plasma mass spectrometry (ICP-MS; NexION 5000, PerkinElmer). Detailed information about the instrumental parameters, calibration protocols, and quality control procedures are outlined in Ge et al. (2024). Quantification was performed using external calibration curves from multi-element standards in 1 M HNO_3, with indium (In) serving as an internal standard to account for instrumental drift. All data underwent rigorous blank correction; detailed blank values are documented in Table S2 in Supporting Information S1.

2.3. Air Mass Back Trajectories

7-day back trajectories of air masses were calculated from initial altitudes of 250, 500, and 1,000 m above sea level, using meteorological input from the Global Data Assimilation System (GDAS; http://arlftp.arlhq.noaa.gov/pub/archives/, 2006- present). For each sampling event, the endpoints of air masses back trajectory were assigned to geographic coordinates corresponding to the initiation, midpoint, and termination of the sampling transect, respectively.

2.4. Evaluation of Enrichment Levels

Enrichment factors (EFs) were used to evaluate the relative enhancement of aerosol-borne TEs compared to crustal abundance, calculated as:

$$\mathrm{EF}_{(\mathrm{TEs})} = \left(\frac{\mathrm{TEs}}{\mathrm{Al}}\right)_{\mathrm{sample}} \Big/ \left(\frac{\mathrm{TEs}}{\mathrm{Al}}\right)_{\mathrm{UCC}} \quad (1)$$

where $\left(\frac{\mathrm{TEs}}{\mathrm{Al}}\right)_{\mathrm{sample}}$ and $\left(\frac{\mathrm{TEs}}{\mathrm{Al}}\right)_{\mathrm{UCC}}$ represent the TE/Al ratios in the aerosol sample and the upper continental crust (UCC; Rudnick & Gao, 2003). EF values near 1 suggest a dominant crustal (mineral dust) origin, whereas values > 10 indicate significant contributions from non-crustal, primarily anthropogenic, sources (Duce et al., 1975).

2.5. Deposition Flux Assessment

The bulk deposition flux (F_{bulk}) of TEs, including both wet and dry deposition, was estimated following the method of Kadko et al. (2020):

$$F_{\mathrm{bulk}} = C_{\mathrm{TEs}} \times V_b$$

$$V_b = 999 \times \text{annual rain rate} + 1040 \text{ m d}^{-1}$$

$$\text{Annual rain rate} = 12 \times \text{monthly average rain rate}$$

$$\text{Monthly average rainrate} = \sum \mathrm{RR}_i \times f_i \times \exp(-\lambda t_i) / \sum f_i \times \exp(-\lambda t_i) \quad (2)$$

Here, V_b (m d^{-1}) is the bulk deposition velocity; RR_i (m $month^{-1}$) denotes the precipitation rate in month i, obtained from ERA5 reanalysis data (https://cds.climate.copernicus.eu/); t_i is the number of days between the first day of month i and the sampling date; and f_i ($0 \leq f_i \leq 1$) is the fraction of the month i during the month of sampling; the annual rain rate (m $year^{-1}$) was calculated using data from the sampling month and the previous 3 months.

3. Result

3.1. Spatial Distribution of Trace Element Concentrations

Aerosol TE concentrations demonstrated notable spatial variability across the AO, with Se exhibiting the largest range (270-fold difference, Figure 2; Table S3 in Supporting Information S1). In the AO, elevated concentrations of most TEs occurred at stations A21 and A22 near Murmansk, Russia, likely due to continental outflow influences. Notably, substantial levels of TEs were also identified at high AO stations A14 and A15, with the air mass backward trajectories did not intersect low-latitude terrestrial regions (Figure 1; Figure S1 in Supporting Information S1).

In order to facilitate a clearer evaluation of TE spatial variability, the study area was divided at 82°N into the Central Arctic Ocean (CAO; A13–A20, A23–A27) and the Peripheral Arctic Ocean (PAO; A8–A12, A28–A29). Stations A21 and A22 were excluded from statistical classification due to their proximity to coastal areas, which may compromise their representativeness of typical Arctic aerosol conditions. Contrary to initial expectations (Duce et al., 1991; Jickells et al., 2005), the CAO did not exhibit significantly lower concentrations of crustal and anthropogenic TEs compared to the PAO, despite its increased distance from terrestrial emission sources. Differences in mean concentrations of these TEs between the CAO and PAO were relatively minor, within a factor of 1.6-fold, with no statistically significant differences observed in TE concentrations between these two regions ($p > 0.05$). Elements including Al (PAO vs. CAO: 17.4 ± 12.2 vs. 16.0 ± 16.3 ng m^{-3}), Ti (2.15 ± 2.44 vs. 1.78 ± 2.65 ng m^{-3}), Mn (0.476 ± 0.363 vs.0.354 ± 0.466 ng m^{-3}), Co (10.3 ± 5.92 vs. 8.20 ± 7.60 pg m^{-3}), Cr (487 ± 390 vs.356 ± 361 pg m^{-3}), Ni (298 ± 225 vs. 257 ± 327 pg m^{-3}), Zn (2.52 ± 1.35 vs.1.67 ± 1.18 ng m^{-3}), and Se (20.0 ± 20.3 vs. 12.8 ± 12.0 pg m^{-3}) were found to have slightly higher (1.1–1.5 times) mean concentrations in the PAO. Surprisingly, Fe (PAO vs. CAO: 14.3 ± 13.1 vs. 16.0 ± 28.7 ng m^{-3}), V (20.1 ± 12.7 vs. 24.9 ± 27.2 pg m^{-3}), As (19.3 ± 13.1 vs.21.3 ± 42.7 pg m^{-3}), Cd (9.54 ± 4.37 vs. 10.1 ± 6.41 pg m^{-3}), and Pb (68.1 ± 33.9 vs. 80.0 ± 74.7 pg m^{-3}) were found to have even slightly higher (1.1–1.2 times) mean concentrations in the CAO.

In comparison with aerosol samples from the Northwest Pacific marginal seas (NWPMS; A1–A7, A30), the AO generally showed lower TE concentrations. Crustal elements, notably Al, showed a reduction of ∼2.4-fold in the AO relative to the NWPMS ($p < 0.05$). The decline in concentrations of anthropogenic TEs was even more pronounced, highlighting the diminished influence of specific anthropogenic sources in the Arctic. Notably, V, an indicator of ship emissions (Schlesinger et al., 2017), was found to have the largest geographical difference, with mean values 12-fold lower in the AO than in the NWPMS ($p < 0.05$), reflecting significant differences in source contributions.

3.2. Element Enrichment Analysis

Fe exhibited crustal-like ratios, with a mean EF less than 2, while Ti, Co, and Mn showed slight enrichment, with a mean EF of 2–3 (Equation 1; Figure 2). In contrast, Cr, Ni, Zn, As, Se, Cd, and Pb were significantly enriched, with EFs ranging tens to over a thousand, indicating considerable anthropogenic contributions. While several TEs exhibited relatively low average EF values, there was notable spital variability; for instance, Ti reached an EF of 5.0 in the PAO, and Fe peaked at 3.4 in the CAO, reflecting the regional heterogeneity of Arctic aerosol.

The mean EFs were comparable between the PAO and CAO, differing by less than 1.4-fold (Figure 3). In comparison to the NWPMS, the AO generally revealed lower elemental enrichments (Figures 2 and 3). Notably, V was significantly enriched within the NWPMS (with a maximum EF of 15 in the Sea of Japan), whereas it remained at low enrichment levels in the AO. Similarly, Mn and Co showed EFs that were 2.7 and 2.0-fold lower, respectively, whereas Fe was 1.1-fold lower, in the Arctic region. An exception was observed for Ti, which was slightly higher enrichment in the AO (1.3-fold). The highly enriched elements displayed EFs that were 1.6- to 3.1-fold lower in the AO compared to the NWPMS, except for Cd and Cr, which maintained comparable enrichment

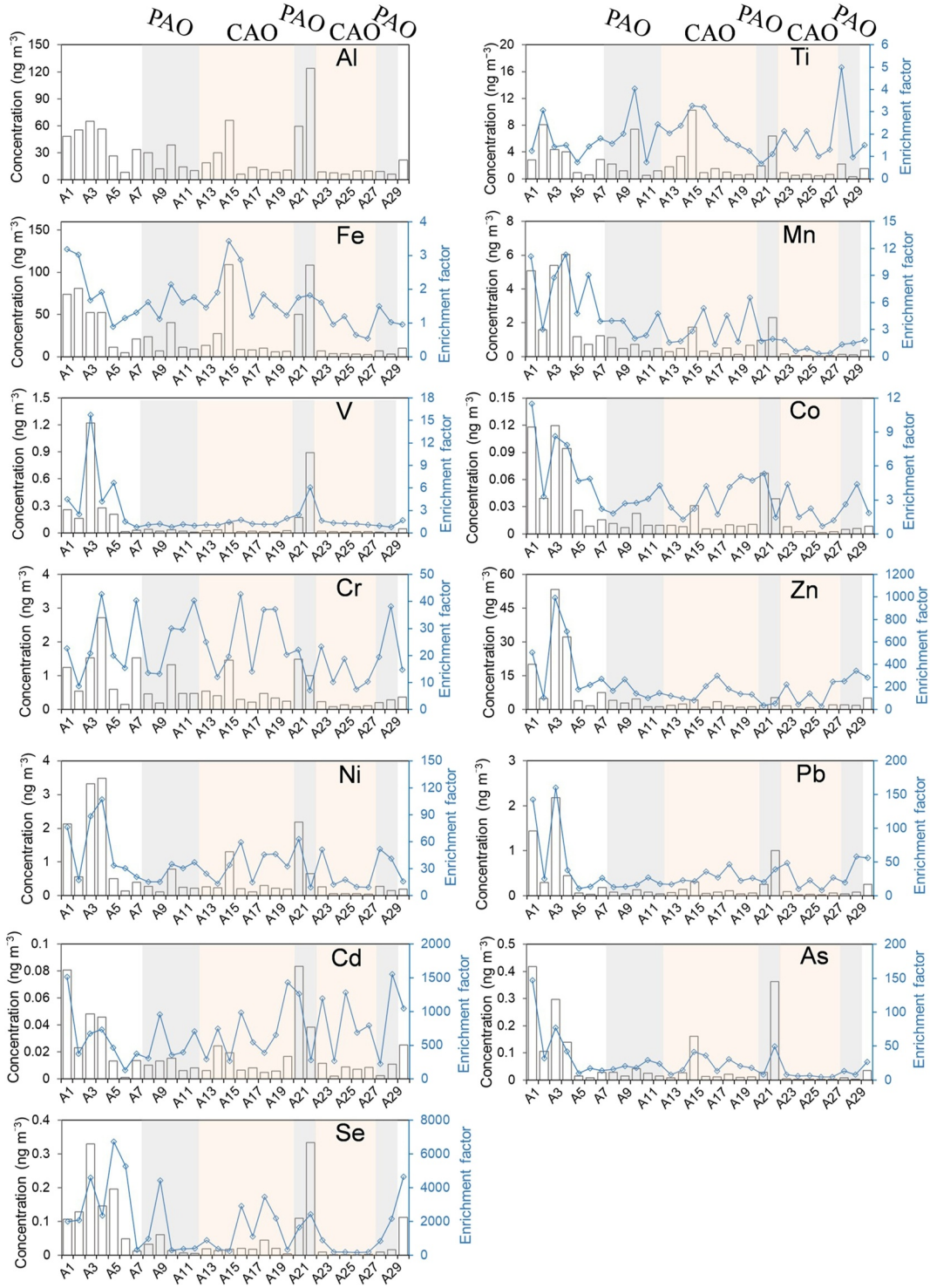

Figure 2. Spatial distribution of trace element concentrations and their enrichment factors in aerosol samples. The gray-shaded area represents the Peripheral Arctic Ocean (PAO) region (<82°N; samples A8–A12, A21–A22, A28, A29), the brown-shaded area indicates the Central Arctic Ocean (CAO) region (>82°N; samples A13–A20, A23–A27), and the unshaded area corresponds to the Northwestern Pacific marginal sea (NWPMS; samples A1–A7, A30) region.

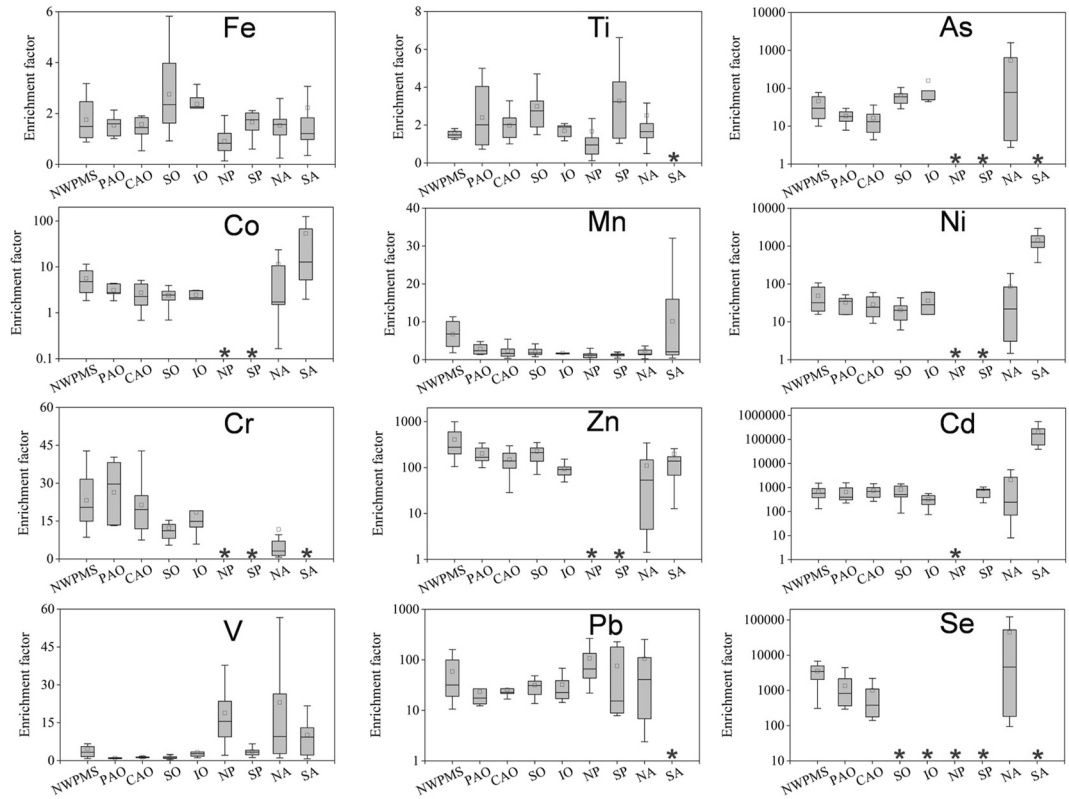

Figure 3. Comparison of trace element enrichment factors among marine basins. NWPMS: Northwestern Pacific marginal sea (this study); PAO: Peripheral Arctic Ocean (this study); CAO: Central Arctic Ocean (this study); SO: Southern Ocean (Ge et al., 2024); IO: Indian Ocean (Ge et al., 2024); NP: North Pacific (Buck et al., 2013); SP: South Pacific (Buck et al., 2019); NA: North Atlantic (Shelley et al., 2015, 2017); SA: South Atlantic (GEOTRACES GA10 Cruise, data from GEOTRACES Intermediate Data Product Group (2023). In the figure, asterisks denote missing values; in the box plot, the solid black line inside the rectangle indicates the median, while blue squares represent the mean.

levels. These findings highlight the complex and generally reduced anthropogenic influence on aerosol TEs in the remote AO compared to the heavily impacted NWPMS.

4. Discussion

4.1. Globally Low Concentrations and Enrichment Deficits of Arctic Aerosol Trace Elements

The AO exhibits depleted concentrations of the dust tracer element Al (Table 1), with levels approximately 50-fold lower than the North Atlantic (Shelley et al., 2015, 2017), and this depletion persists across the North Pacific (Buck et al., 2013), South Pacific (Buck et al., 2019), Indian Ocean (Ge et al., 2024), and South Atlantic (GEOTRACES Intermediate Data Product Group, 2023), but comparable to the remote Southern Ocean (Ge et al., 2024). Similarly, TEs with low crustal EFs, such as Mn, Ti, and Co, demonstrate consistently reduced distributions. At the extremes for Fe and V, which exhibit the lowest global mean concentrations within the AO. Collectively, these patterns indicate that mineral-dominated TEs in the AO occupy the lower extreme of global oceanic concentration ranges.

Concentrations of most anthropogenic TEs are similarly depressed in the AO, compared with observations from other ocean basins (Table 1). As and Pb register the lowest Arctic concentrations globally—2.8-fold and 1.6-fold lower, respectively, than the second-lowest means observed in the Southern Ocean (Ge et al., 2024). Ni, Zn, and Cd exhibit the second-lowest Arctic concentrations: Ni marginally exceeds Southern Ocean values, while Zn and Cd exceed Indian Ocean concentrations, but remain lower than all other oceans. Conversely, Cr shows moderate concentrations, with Arctic levels approximately 2-fold and 1.5-fold higher than the Southern Ocean and Indian Ocean, respectively.

Journal of Geophysical Research: Atmospheres

10.1029/2025JD045561

Table 1
Aerosol Trace Element Concentrations in the Arctic Ocean and Northwestern Pacific Marginal Seas Compared With Historical Basin-Scale Studies

Ocean regions	Al[a]	Ti[a]	Fe[a]	Mn[a]	Zn[a]	V[b]	Co[b]	Cr[b]	Ni[b]	As[b]	Se[b]	Cd[b]	Pb[b]	References
Arctic Ocean	16.5 (14.7)	1.91 (2.52)	15.4 (24.0)	0.397 (0.427)	1.96 (1.28)	23.2 (22.9)	8.92 (6.97)	402 (367)	272 (289)	20.6 (34.7)	15.3 (15.3)	9.93 (5.66)	75.8 (62.6)	this study
Central Arctic Ocean	16.0 (16.3)	1.78 (2.65)	16.0 (28.7)	0.354 (0.466)	1.67 (1.18)	24.9 (27.2)	8.20 (7.60)	356 (361)	257 (327)	21.3 (42.7)	12.8 (12.0)	10.1 (6.41)	80.0 (74.7)	this study
Peripheral Arctic Ocean	17.4 (12.2)	2.15 (2.44)	14.3 (13.1)	0.476 (0.363)	2.52 (1.35)	20.1 (12.7)	10.3 (5.92)	487 (390)	298 (225)	19.3 (13.1)	20.0 (20.3)	9.54 (4.37)	68.1 (33.9)	this study
Northwest Pacific marginal seas	39.4 (19.9)	3.15 (2.41)	38.3 (30.3)	2.70 (2.36)	16.0 (18.3)	278 (395)	53.7 (48.6)	1080 (849)	1340 (1410)	131 (151)	135 (97.1)	31.5 (25.6)	608 (778)	this study
Arctic Ocean	16.2 (12.1)	1.11 (1.01)	4.49 (5.22)	0.081 (0.121)	2.11 (1.60)	13.8 (18.5)	3.66 (3.53)	239 (213)	89.8 (52.5)			355 (285)	430 (349)	Marsay, Kadko, et al. (2018)
Central Arctic Ocean	11.0 (7.17)	1.68 (1.92)	32.0 (16.8)	0.350 (0.190)	2.93 (2.40)	12.8 (14.1)	22.7 (15.9)	320 (341)	434 (497)			237 (349)	457 (559)	Kadko et al. (2016)
Southern Ocean	16.1 (9.61)	2.20 (1.48)	22.8 (19.7)	0.329 (0.269)	3.05 (2.78)	27.9 (23.9)	7.91 (5.40)	202 (112)	184 (157)	59.2 (56.6)		11.8 (16.5)	101 (74.0)	Ge et al. (2024)
Indian Ocean	22.9 (12.8)	1.86 (1.02)	27.5 (16.5)	0.415 (0.329)	1.91 (1.52)	78.7 (54.9)	11.9 (8.48)	365 (164)	419 (341)	120 (86.5)		8.30 (7.29)	184 (176)	Ge et al. (2024)
North Atlantic	806 (1680)	63.9 (133)	6220 (1290)	10.7 (22.0)	3.13 (4.15)	2400 (4130)	283 (560)	1410 (2570)	1190 (1540)	411 (355)	460 (332)	44.7 (60.5)	867 (1220)	Shelley et al. (2015, 2017)
South Atlantic	24.7 (24.6)		17.5 (18.9)	0.749 (0.620)	2.83 (3.34)	163 (135)	89.8 (76.7)		5730 (3490)			1450 (1080)		GEOTRACES Intermediate Data Product Group (2023)
North Pacific	73.2 (93.3)	5.48 (8.81)	37.2 (59.0)	1.15 (1.88)		1100 (726)							3550 (5590)	Buck et al. (2013)
South Pacific	26.0 (52.3)	1.80 (2.68)	17.6 (33.3)	0.334 (0.651)		150 (294)						18.8 (30.1)	245 (276)	Buck et al. (2019)

Note. Values in parentheses denote $\pm 1\sigma$ standard deviation of sample concentrations. [a]indicates units of ng m^{-3}, while. [b]denotes pg m^{-3}.

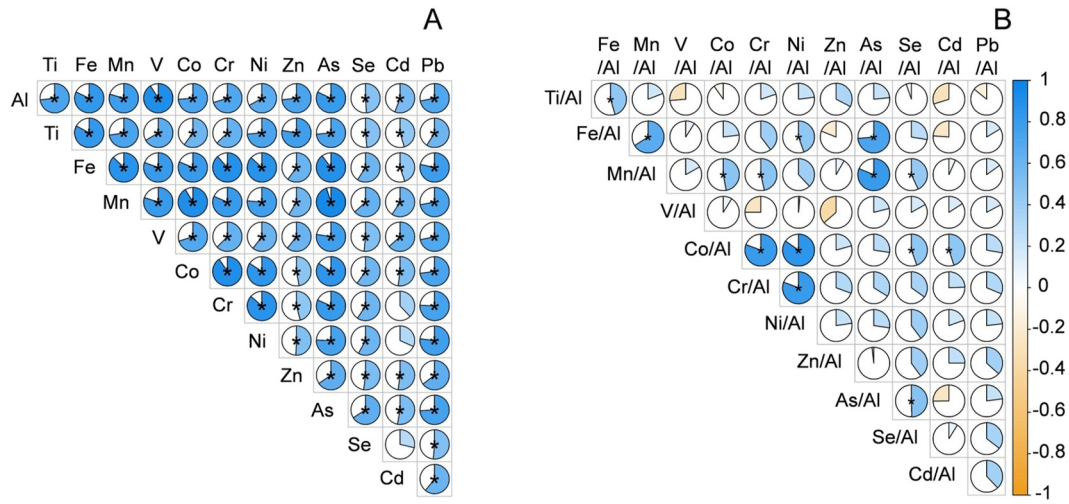

Figure 4. Spearman correlation analysis of trace elements (TEs) in Arctic Ocean aerosols. Panel (a) illustrates correlations between TE concentrations, while Panel (b) demonstrates correlations among Al-normalized TE concentrations (TEs/Al). In the pie charts, the area and color intensity represent the magnitude of correlation coefficients, with asterisks (*) denoting statistically significant relationships ($P < 0.05$).

Compared to global oceanic basins, the AO demonstrates systematically lower EFs for most aerosol TEs (e.g., Ni, Zn, Cd, and As), with V, Pb, and Se registering the lowest EFs globally (Figure 3). Notably, the AO recorded the lowest V concentrations and enrichment levels observed in global oceans, reflecting minimal influence from shipping activities. Meanwhile, most mineral-dominated TEs (Ti, Fe, Co) exhibit intermediate enrichment, whereas mineral-dominated Mn and anthropogenic Cr show notable elevated EFs. The subdued enrichment and concentration level of anthropogenic TEs reflects relatively limited pollutant transport to the Arctic, except for Cr, which shows stronger anthropogenic contributions. For mineral-dominated TEs (Ti, Fe, Co, Mn), their intermediate or elevated enrichment distributions likely result not only from natural aerosol fractionation but also anthropogenic influences. These anthropogenic influences are matched with our observations and historical investigations in Northern Hemisphere oceans (Shelley et al., 2015, 2017): EFs of Fe, Mn, and Co in the AO are generally lower than those in the NWPMS, while Fe, Ti, Mn, and Co levels are comparable to or lower than those in the North Atlantic. This implies that long-range transport of industrial aerosols may drive their relative enrichment in Arctic regions.

4.2. Anthropogenic Perturbations to the Arctic Ocean Trace Element Distributions

Spearman correlation analysis revealed strong associations ($r = 0.73$–0.82; Figure 4a) between low-EF TEs (Fe, Mn, Co, Ti) and the dust tracer Al, reconfirming the dominant contribution of mineral sources to these TEs in Arctic aerosols. Notably, V displayed its strongest association with Al ($r = 0.91$), contradicting its typical role as a ship-emission tracer (Schlesinger et al., 2017), suggesting a currently relatively limited influence from maritime traffic in the AO. High-EF TEs also showed significant correlations with Al, particularly As, a species with a stronger relationship ($r = 0.82$) than most low-EF species, indicating effective mixing process of anthropogenic and mineral aerosols. Additionally, the superior inter-element correlations among certain low-EF TEs than with Al (e.g., Ti-Fe > Ti-Al) suggest natural fractionation processes or supplemental non-crustal inputs. Furthermore, the highly variable correlations among High-EF TEs reveal multiple anthropogenic sources. These findings highlight the complexity of aerosol sources in the Arctic, where long-range transport of mixed continental air masses coexists with localized particles emission.

Al-normalized TE concentrations (Figure 4b), which minimizing atmospheric processing effects (Ge et al., 2024; Kurisu et al., 2024), were analyzed to further identify intrinsic elemental relationships. Coal combustion tracers Se and As (Se/Al vs. As/Al) showed strong correlations (Shen et al., 2024), confirming coal-derived emissions influence on Arctic aerosols. Contrary to expectations, conventional ship emission tracers Ni and V (Ni/Al vs. V/Al) showed weak correlations with atypical V/Ni ratios (generally 0.04–0.25; excepting Sample A22 near Murmansk, Russia, at 1.4) notably diverging from the characteristic ship emission ranges (0.5–3.0) (Becagli

et al., 2020; Yu et al., 2021; Zhao et al., 2021). Globally, the North Atlantic exhibits the highest Ni/V ratio of 1.49 ± 0.96 (Shelley et al., 2015, 2017), falling within the range of ship emissions and suggesting their influence. In contrast, other ocean basins show significantly lower V/Ni ratios relative to typical ship emission values: the Indian Ocean at 0.22 ± 0.15 (Ge et al., 2024), NWPMS at 0.21 ± 0.13, the Southern Ocean at 0.20 ± 0.29 (Ge et al., 2024), CAO at 0.13 ± 0.07, PAO at 0.08 ± 0.05, and the South Atlantic at 0.03 ± 0.03 (GEOTRACES Intermediate Data Product Group, 2023). Ni (Ni/Al) exhibited its strongest association with Cr (Cr/Al), while Ni/Al demonstrating no significant linkages to metallurgical- dominant tracer (Zn/Al) (Wei et al., 2025) or coal combustion tracers (As/Al, Se/Al)—a pattern consistent with nonexhaust vehicular emissions, as both elements are extensively utilized in automotive brake linings, an increasingly significant class of traffic-related particle emissions (Neukirchen et al., 2025; Thomas et al., 2024).

Pb displayed broad correlations with anthropogenic TEs in raw concentrations that dissipated following Al-normalization, potential influence from multiple anthropogenic sources. Cd demonstrated selective associations solely with Zn, As, and Pb in unnormalized data—linkages that similarly vanished post-normalization—revealing complex source heterogeneity potentially stemming from coupled metallurgical emissions and coal combustion influences, or other anthropogenic sources.

Notably, even low-EF TEs exhibited significant ties to post-Al-normalization anthropogenic species (e.g., Fe/Al-As/Al, Mn/Al-As/Al, and Co/Al-Cr/Al ratios), revealing unexpected anthropogenic perturbations on these conventional mineral TE distributions in this remote Arctic marine environment. These signatures likely reflect coal combustion impacts on Fe/Mn and vehicular emission influences on Co cycles, suggesting anthropogenic imprints in polar regions.

4.3. Decadal Comparison of Trace Element Variation Trends in the Summer Arctic Ocean

This study implemented strictly controlled wind-based sampling following GEOTRACES protocols, enabling decadal comparisons with the GEOTRACES GA10 campaign (09 August–12 October 2015; Marsay, Kadko, et al., 2018), ARK-XXVI/3 campaign (13 August–21 September 2011; Kadko et al., 2016) and IAOE-91 campaign (1 August–6 October 1991; Maenhaut et al., 1996). Our latitudinal data show comparable mean Al concentrations in CAO and PAO (Table 1), and Marsay, Kadko, et al. (2018) reported a 1.6-fold higher CAO levels (Figure 5), indicating stable or intensified mineral dust concentration across higher Arctic latitudes regardless of continental proximity. Consistently, both data sets indicate the predominant influence of Arctic circumpolar air mass transport during observation periods, effectively isolating the CAO from direct low-latitude continental inputs. In contrast, localized emissions from surface sea snow/ice resuspension are likely central to elevated mineral dust concentrations. This process incorporates post aerosol-deposited or shelf-transported mineral materials (Bolt et al., 2020; Gao et al., 2019; Marsay, Aguilar-Islas, et al., 2018), implicating the sea ice system as a potential source of TEs to open AO waters via aerosol deposition. The high mineral Al and Fe concentrations in the ice zone were also recorded during the summer cruise observations in 1991 (Figure 5), for example, the Al median in PM_{10} was 9.3 ng m^{-3} in the ice-free zone and 14.0 ng m^{-3} in the ice zone (Maenhaut et al., 1996). This significant deviation from conventional mineral dust distribution model predictions (Duce et al., 1991; Jickells et al., 2005), compels an urgent reassessment of dust transport frameworks using observational data, given the Arctic accelerated environmental changes.

For anthropogenic TEs Cr, Ni, and Zn, EFs showed stable decadal patterns (Figure 5). Previous studies found no significant V enrichment in summer 2014 (EF: 0.67 ± 1.42) or summer 2011 (EF: 0.82 ± 0.41) (Kadko et al., 2016; Marsay, Kadko, et al., 2018), but this study observed a near two-fold increase in V concentrations (Table 1) and EFs (EF: 1.21 ± 0.297). This modest increase is potentially linked to the exponentially growing maritime traffic in the rapidly intensifying Arctic navigation corridor, while remaining below significant levels, as the post-increase V EF remains low. Notably, the concentrations of Pb and Cd exhibited dramatic plummets, decreasing 6-fold and 35-fold respectively (Table 1; Figure 5), while their EFs obediently retreated by nearly an order of magnitude (Marsay, Kadko, et al., 2018). The substantial reduction in Pb is consistent with recent observations in the Southern Ocean (Ge et al., 2024), suggesting the effectiveness of improved emission regulations in related source regions.

Kadko et (2016) reported remarkably high Fe EFs in the CAO, with Al-normalized EFs reaching 15, and Ti, Mn, and Co exhibited EFs greater than 1. This study also observed Fe, Ti, Mn, and Co enrichment patterns but with lower mean EFs than Kadko et al. (2016). This contrasts with Marsay, Kadko, et al. (2018) reporting

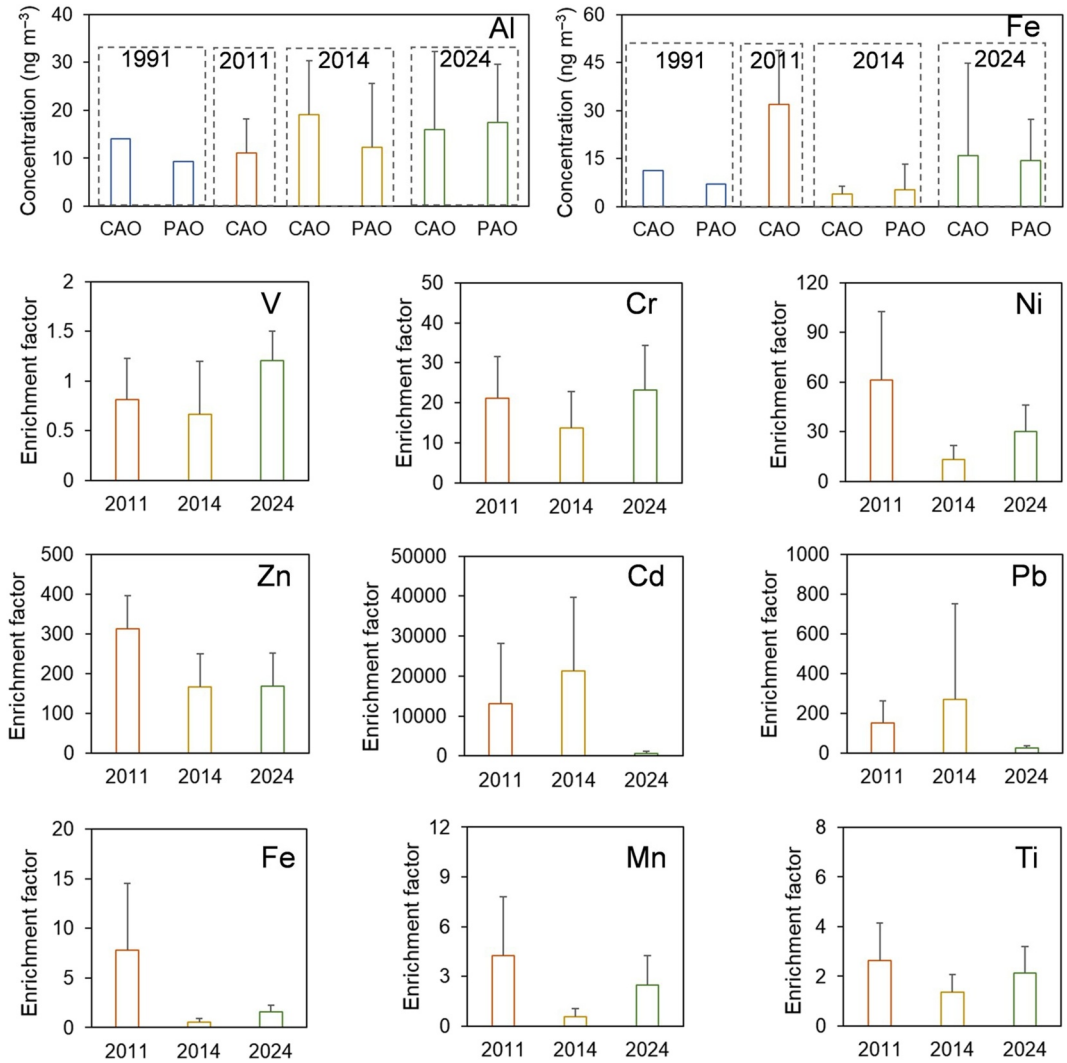

Figure 5. Comparative analysis of trace element (Al, Fe) concentrations and enrichment factors (V, Cr, Ni, Zn, Cd, Pb, Fe, Mn, Ti) in the Arctic Ocean over the past decade, incorporating data from four key studies: This study (19 July to 24 September 2024), Marsay, Kadko, et al. (2018) (GEOTRACES GA10 campaign conducted 9 August to 12 October 2015), Kadko et al. (2016) (ARK-XXVI/3 campaign spanning 13 August to 21 September 2011), and Maenhaut et al. (1996) (IAOE-91 campaign from 1 August to 6 October 1991). Special consideration is given to methodological variations, particularly that Maenhaut et al. (1996) measured PM_{10} concentrations whereas other studies analyzed total suspended particulates. For spatial consistency, the pack ice region in Maenhaut et al. (1996) has been reclassified as Central Arctic Ocean (CAO) and their ocean subset as Peripheral Arctic (PCA) in our current framework.

predominantly sub-unity EFs for Fe and Mn. These discrepancies suggest complex Arctic aerosol source dynamics. While mineral dust is the primary source of low-EF TEs, regional and annual variations exist, and the key controlling factors remain poorly constrained. One of the possible reasons for the depletion of Fe relative to Al is thawing permafrost (Gao et al., 2019; Pokrovsky et al., 2018; Sebaaly et al., 2025). This process exposes mineral soils with characteristically low Fe/Al ratios as Fe is preferentially lost over Al, while resuspension processes of weathered permafrost particles may preferentially deplete Fe in aerosols. However, in this study, the significant correlations between Fe/Al, Mn/Al ratios and several anthropogenic TEs/Al imply potential human contributions that may mask the Fe depletion signals caused by permafrost weathering. This suggests that the Fe in Arctic aerosols may be in a dynamic balance between depletion and enrichment, influenced by the interaction of local continental/sea ice surface permafrost particles and long-range transported anthropogenic and mineral Fe sources.

Table 2
The Mean Values (±1σ in Parentheses) of the Evaluated Bulk Deposition Fluxes for Aerosol Trace Elements (ng m^{-2} d^{-1}) and Dust (mg m^{-2} d^{-1}) Are Presented for the Arctic Ocean, Central Arctic Ocean, Peripheral Arctic Ocean, and the Northwestern Pacific Marginal Seas

	Arctic Ocean	Central Arctic Ocean	Peripheral Arctic Ocean	Northwestern Pacific marginal seas
Al	23900 (20700)	24300 (23800)	23100 (14800)	79800 (48800)
Ti	2740 (3540)	2680 (3890)	2850 (3080)	6240 (4830)
Fe	22200 (34800)	24000 (42000)	18800 (16200)	77600 (63500)
Mn	567 (606)	536 (690)	626 (453)	5660 (5440)
V	33.9 (33.2)	37.9 (39.7)	26.5 (15.4)	627 (1010)
Co	12.9 (9.75)	12.5 (11.2)	13.7 (7.13)	114 (114)
Cr	577 (501)	539 (526)	649 (483)	2170 (1800)
Ni	393 (411)	389 (479)	400 (279)	2880 (3260)
Zn	2830 (1700)	2540 (1730)	3370 (1620)	35000 (45200)
As	29.6 (50.8)	31.8 (62.7)	25.4 (16.2)	281 (340)
Se	21.9 (20.7)	19.3 (18.0)	26.6 (25.9)	282 (247)
Cd	14.7 (8.38)	15.7 (9.63)	12.8 (5.57)	65.2 (57.1)
Pb	111 (91.1)	122 (109)	91.9 (42.4)	1350 (1910)
Dust	0.295 (0.255)	0.300 (0.294)	0.285 (0.183)	0.985 (0.603)

Note. The dust flux was calculated based on Al concentrations in aerosols and the crustal abundance of Al in the upper continental crust.

4.4. Bulk Flux Assessment of Dust and Trace Elements

The bulk deposition fluxes of dust and TEs were calculated using aerosol bulk deposition velocity derived from precipitation data inversion (Equtaion 2, Table 2; Kadko et al., 2020). This study determined a mean bulk deposition velocity of 1,480 ± 122 m d^{-1} in the AO. This value is approximately 1.5 times higher than the typical dry deposition velocity of 1,000 m d^{-1} for bulk mineral aerosols, indicating relatively limited contribution from wet deposition processes. Based on aerosol Al concentrations and its UCC abundance (8.1%; Rudnick & Gao, 2003), the bulk dust flux across the AO was estimated to range from 0.113 to 1.20 mg m^{-2} d^{-1}, with a median value of 0.199 mg m^{-2} d^{-1}. This estimate aligns well with Marsay, Kadko, et al. (2018) observations in Western AO (range: 0.030–0.499 mg m^{-2} d^{-1}; median: 0.142 mg m^{-2} d^{-1}). Spatially, the mean flux in the AO was 0.295 ± 0.255 mg m^{-2} d^{-1}, which is 3.3 times lower than the estimated flux for the NWPMS. In contrast, dust fluxes in the CAO and PAO showed comparable magnitudes (Table 2). Globally, the bulk dust flux in the AO is substantially lower than values reported for the Indian Ocean (0.837 ± 0.700 mg m^{-2} d^{-1}; Ge et al., 2024) and the South Pacific (0.477 ± 0.181 mg m^{-2} d^{-1}; Buck et al., 2019). While comparable to fluxes in the Southern Ocean's Pacific and Indian sectors (0.302 ± 0.187 mg m^{-2} d^{-1}; Ge et al., 2024), it maintains a 1.9-fold elevation over the remote central North Pacific (0.157 ± 0.088 mg m^{-2} d^{-1}; Marsay, Kadko, et al., 2018). Collectively, this systematic quantification positions the Arctic deposition regime within the lowest quintile of global dust flux distribution.

The mean bulk Fe deposition flux in the CAO (24.0 ± 42.1 μg m^{-2} d^{-1}) notable exceeded the PAO value (18.8 ± 16.2 μg m^{-2} d^{-1}). A slightly elevated spatial flux pattern was also observed for Al, V, As, Cd, and Pb in the CAO. The weaker lithogenic signature in off-shelf Arctic seawater (Kanna et al., 2025; Zhang et al., 2021) and elevated aerosol Fe fluxes jointly imply greater aerosol deposition influences to surface Fe budgets in the CAO than PAO. The cryptic transfer facilitated by the synergistic coupling of ice/snow resuspension with aerosol deposition processes collectively enhances TE redistribution in the Arctic marine system. Additionally, current Arctic warming, characterized by extensive sea ice retreat and permafrost thawing, may reorganize these summer flux patterns, modifying air-sea TE exchanges. Furthermore, pronounced Fe/Al fractionation in summer Arctic aerosols, driven by the interplay between local emissions and long-distance anthropogenic transport, introduces important bias in dust-based Fe flux estimation (a 2.7-fold difference of mean Fe/Al value between this study and Marsay, Kadko, et al. (2018)). This reveals the complexity of Arctic aerosol transformations under rapid climate

change, necessitating refinement of climate models for aerosol-climate quantification. Thus, advancing the understanding of present-day and future Arctic biogeochemical cycles requires more detailed knowledge of aerosol TE spatial distribution, enrichment mechanisms, and deposition fluxes.

5. Conclusions

This study provides new insights into aerosol TEs in the rapidly warming AO through an integrated analysis of spatial patterns, anthropogenic fingerprints, and flux assessments, yielding the following key conclusions. First, the spatial homogeneity of TE concentrations between the CAO and PAO was relatively minor, with mean concentration differences typically below 1.6-fold. Notably, comparable or even higher Fe and Al concentrations in the CAO contradict dust models, suggesting a potential role for local resuspension from sea ice/snow. Second, source apportionment unequivocally identifies coal combustion for As and Se, non-exhaust vehicle emissions for Ni and Cr, metallurgical sources for Zn, and mixed anthropogenic origins for Pb and Cd, whereas mineral sources dominate Fe, Ti, Mn, Co, and V, albeit with detectable anthropogenic influences. Crucially, both TE concentrations and anthropogenic enrichment levels in the Arctic aerosol generally rank among the lower ends observed globally. Third, decadal comparisons reveal divergent anthropogenic trajectories: a remarkable order-of-magnitude decline for Pb and Cd, contrasting with stable enrichment for Ni, Cr, As, Se, and Zn. Emerging Arctic shipping activity is now reshaping V profiles. The pronounced fractionation of Fe relative to Al exhibits alternating depletion and enrichment patterns, likely driven by the mixing between anthropogenic Fe-rich particles and thawed permafrost weathered Fe-depleted particles. Fourth, the summer dust and Fe bulk deposition fluxes are 0.295 ± 0.255 mg m^{-2} d^{-1} and 22.2 ± 34.8 μg m^{-2} d^{-1}, respectively, positioning the region at the lower end of global estimates. A pivotal finding is the higher Fe flux in the CAO compared to PAO, offering critical constraints for models. Furthermore, pronounced Fe/Al fractionation introduces substantial uncertainty in Fe flux assessments. These findings reveal the unique distribution and source characteristics of TEs in Arctic aerosols, strengthen the understanding of TE cycling amid accelerating Arctic warming, and contribute significantly to advancing polar climate science and environmental prediction.

Conflict of Interest

The authors declare no conflicts of interest relevant to this study.

Data Availability Statement

All data supporting this study are available in Tables S1 and S3 in Supporting Information S1, with the complete data set archived in the Zenodo repository at https://doi.org/10.5281/zenodo.17878667.

Acknowledgments
We are grateful to the captain and the crew of the oceanographic research vessel Xue Long 2 for their invaluable support in installing equipment and assisting with the sampling process. We acknowledge Dr. Shen Shan for his assistance in aerosol collection from the First Institute of Oceanography, MNR (FIO). This research was supported by the Natural Science Foundation of China (Grants 42576265, 42330412, 42506256).

References

Becagli, S., Caiazzo, L., Di Iorio, T., di Sarra, A., Meloni, D., Muscari, G., et al. (2020). New insights on metals in the Arctic aerosol in a climate changing world. *Science of the Total Environment*, *741*, 140511. https://doi.org/10.1016/j.scitotenv.2020.140511

Bolt, C., Aguilar-Islas, A., & Rember, R. (2020). Particulate trace metals in Arctic snow, sea ice, and underlying surface waters during the 2015 US western Arctic GEOTRACES cruise GN01. *ACS Earth and Space Chemistry*, *4*(12), 2444–2460. https://doi.org/10.1021/acsearthspacechem.0c00208

Browning, T. J., & Moore, C. M. (2023). Global analysis of ocean phytoplankton nutrient limitation reveals high prevalence of co-limitation. *Nature Communications*, *14*(1), 5014. https://doi.org/10.1038/s41467-023-40774-0

Buck, C. S., Aguilar-Islas, A., Marsay, C., Kadko, D., & Landing, W. M. (2019). Trace element concentrations, elemental ratios, and enrichment factors observed in aerosol samples collected during the US GEOTRACES eastern Pacific Ocean transect (GP16). *Chemical Geology*, *511*, 212–224. https://doi.org/10.1016/j.chemgeo.2019.01.002

Buck, C. S., Landing, W. M., & Resing, J. (2013). Pacific Ocean aerosols: Deposition and solubility of iron, aluminum, and other trace elements. *Marine Chemistry*, *157*, 117–130. https://doi.org/10.1016/j.marchem.2013.09.005

Confer, K. L., Jaeglé, L., Liston, G. E., Sharma, S., Nandan, V., Yackel, J., et al. (2023). Impact of changing Arctic sea ice extent, sea ice age, and snow depth on sea salt aerosol from blowing snow and the open ocean for 1980–2017. *Journal of Geophysical Research: Atmospheres*, *128*(3), e2022JD037667. https://doi.org/10.1029/2022JD037667

Danielson, R. E., Zhang, M., & Perrie, W. A. (2020). Possible impacts of climate change on fog in the Arctic and subpolar North Atlantic. *Advances in Statistical Climatology, Meteorology and Oceanography*, *6*(1), 31–43. https://doi.org/10.5194/ascmo-6-31-2020

De Vera, J., Chandan, P., Landing, W. M., Stupple, G. W., Steffen, A., & Bergquist, B. A. (2021). Amount, sources, and dissolution of aerosol trace elements in the Canadian Arctic. *ACS Earth and Space Chemistry*, *5*(10), 2686–2699. https://doi.org/10.1021/acsearthspacechem.1c00132

Duan, L., Song, J., Yin, M., Liu, X., Liu, X., Li, X., & Yuan, H. (2025). Hypoxia exacerbate the marine ecological risk of arsenic: By stimulating its migration and release at the sediment-water interface. *Water Research*, *268*, 122603. https://doi.org/10.1016/j.watres.2024.122603

Duce, R. A., Hoffman, G. L., & Zoller, W. H. (1975). Atmospheric trace metals at remote northern and southern hemisphere sites: Pollution or natural? *Science*, *187*(4171), 59–61. https://doi.org/10.1126/science.187.4171.59

Duce, R. A., Liss, P. S., Merrill, J. T., Atlas, E. L., Buat-Menard, P., Hicks, B. B., et al. (1991). The atmospheric input of trace species to the world ocean. *Global Biogeochemical Cycles*, *5*(3), 193–259. https://doi.org/10.1029/91GB01778

Ducklow, H. W., Steinberg, D. K., & Buesseler, K. O. (2001). Upper ocean carbon export and the biological pump. *Oceanography*, *14*(4), 50–58. https://doi.org/10.5670/oceanog.2001.06

Gao, Y., Marsay, C. M., Yu, S., Fan, S., Mukherjee, P., Buck, C. S., & Landing, W. M. (2019). Particle-size variability of aerosol iron and impact on iron solubility and dry deposition fluxes to the Arctic Ocean. *Scientific Reports*, *9*(1), 16653. https://doi.org/10.1038/s41598-019-52468-z

Ge, Y., Guan, W., Wong, K. H., & Zhang, R. (2024). Spatial variability and source identification of trace elements in aerosols from Northwest Pacific marginal sea, Indian Ocean and South Pacific to Antarctica. *Global Biogeochemical Cycles*, *38*(9), e2024GB008235. https://doi.org/10.1029/2024GB008235

GEOTRACES Intermediate Data Product Group. (2023). *The GEOTRACES Intermediate Data Product 2021 version 2 (IDP2021v2)*. NERC EDS British Oceanographic Data Centre NOC. https://doi.org/10.5285/ff46f034-f47c-05f9-e053-6c86abc0dc7e

He, Y., Inman, H., Kadko, D. C., Stephens, M. P., Hammond, D. E., Landing, W. M., & Mason, R. P. (2025). Elevated methylmercury in Arctic rain and aerosol linked to air-sea exchange of dimethylmercury. *Science Advances*, *11*(12), eadr3805. https://doi.org/10.1126/sciadv.adr3805

Heintzenberg, J., Leck, C., & Tunved, P. (2015). Potential source regions and processes of aerosol in the summer Arctic. *Atmospheric Chemistry and Physics*, *15*(11), 6487–6502. https://doi.org/10.5194/acp-15-6487-2015

Ji, X., Abakumov, E., & Xie, X. (2019). Atmosphere-ocean exchange of heavy metals and polycyclic aromatic hydrocarbons in the Russian Arctic Ocean. *Atmospheric Chemistry and Physics*, *19*(22), 13789–13807. https://doi.org/10.5194/acp-19-13789-2019

Jickells, T. D., An, Z. S., Andersen, K. K., Baker, A. R., Bergametti, G., Brooks, N., et al. (2005). Global iron connections between desert dust, ocean biogeochemistry, and climate. *Science*, *308*(5718), 67–71. https://doi.org/10.1126/science.1105959

Kadko, D., Galfond, B., Landing, W. M., & Shelley, R. U. (2016). Determining the pathways, fate, and flux of atmospherically derived trace elements in the Arctic ocean/ice system. *Marine Chemistry*, *182*, 38–50. https://doi.org/10.1016/j.marchem.2016.04.006

Kadko, D., Landing, W. M., & Buck, C. S. (2020). Quantifying atmospheric trace element deposition over the ocean on a global scale with satellite rainfall products. *Geophysical Research Letters*, *47*(7), e2019GL086357. https://doi.org/10.1029/2019GL086357

Kanna, N., Tateyama, K., Waseda, T., Timofeeva, A., Papadimitraki, M., Whitmore, L., et al. (2025). Spatial distributions of iron and manganese in surface waters of the Arctic's Laptev and East Siberian seas. *Biogeosciences*, *22*(4), 1057–1076. https://doi.org/10.5194/bg-22-1057-2025

Klunder, M. B., Bauch, D., Laan, P., De Baar, H. J., van Heuven, S., & Ober, S. (2012). Dissolved iron in the Arctic shelf seas and surface waters of the central Arctic Ocean: Impact of Arctic river water and ice-melt. *Journal of Geophysical Research*, *117*(C1), 1–18. https://doi.org/10.1029/2011JC007133

Krisch, S., Hopwood, M. J., Roig, S., Gerringa, L. J., Middag, R., Rutgers van der Loeff, M. M., et al. (2022). Arctic–Atlantic exchange of the dissolved micronutrients iron, manganese, cobalt, nickel, copper and zinc with a focus on Fram Strait. *Global Biogeochemical Cycles*, *36*(5), e2021GB007191. https://doi.org/10.1029/2021GB007191

Kurisu, M., Sakata, K., Nishioka, J., Obata, H., Conway, T. M., Hunt, H. R., et al. (2024). Source and fate of atmospheric iron supplied to the subarctic North Pacific traced by stable iron isotope ratios. *Geochimica et Cosmochimica Acta*, *378*, 168–185. https://doi.org/10.1016/j.gca.2024.06.009

Lannefors, H., Heintzenberg, J., & Hansson, H. C. (1983). A comprehensive study of physical and chemical parameters of the Arctic summer aerosol; results from the Swedish expedition Ymer-80. *Tellus B*, *35*(1), 40–54. https://doi.org/10.1111/j.1600-0889.1983.tb00006.x

Maenhaut, W., Ducastel, G., Leck, C., Nilsson, E. D., & Heintzenberg, J. (1996). Multi-elemental composition and sources of the high Arctic atmospheric aerosol during summer and autumn. *Tellus B: Chemical and Physical Meteorology*, *48*(2), 300–321. https://doi.org/10.1034/j.1600-0889.1996.t01-1-00011.x

Mahowald, N. M., Hamilton, D. S., Mackey, K. R., Moore, J. K., Baker, A. R., Scanza, R. A., & Zhang, Y. (2018). Aerosol trace metal leaching and impacts on marine microorganisms. *Nature Communications*, *9*(1), 2614. https://doi.org/10.1038/s41467-018-04970-7

Marsay, C. M., Aguilar-Islas, A., Fitzsimmons, J. N., Hatta, M., Jensen, L. T., John, S. G., et al. (2018). Dissolved and particulate trace elements in late summer Arctic melt ponds. *Marine Chemistry*, *204*, 70–85. https://doi.org/10.1016/j.marchem.2018.06.002

Marsay, C. M., Kadko, D., Landing, W. M., Morton, P. L., Summers, B. A., & Buck, C. S. (2018). Concentrations, provenance and flux of aerosol trace elements during US GEOTRACES Western Arctic cruise GN01. *Chemical Geology*, *502*, 1–14. https://doi.org/10.1016/j.chemgeo.2018.06.007

Masson-Delmotte, V., Zhai, P., Pirani, A., Connors, S. L., Péan, C., Berger, S., et al. (2021). Climate change 2021: The physical science basis. Contribution of working group I to the sixth assessment report of the intergovernmental panel on climate change, *2*(1), 2391. https://doi.org/10.1017/9781009157896

Neukirchen, C., Saraji-Bozorgzad, M. R., Mäder, M., Mudan, A. P., Czasch, P., Becker, J., et al. (2025). Comprehensive elemental and physical characterization of vehicle brake wear emissions from two different brake pads following the Global Technical Regulation methodology. *The Journal of Hazardous Materials*, *482*, 136609. https://doi.org/10.1016/j.jhazmat.2024.136609

Paytan, A., Mackey, K., Chen, Y., Lima, I., Doney, S., Mahowald, N., et al. (2009). Toxicity of atmospheric aerosols on marine phytoplankton. *Proceedings of the National Academy of Sciences of the United States of America*, *106*(12), 4601–4605. https://doi.org/10.1073/pnas.0811486106

Pernov, J. B., Beddows, D., Thomas, D. C., Dall Osto, M., Harrison, R. M., Schmale, J., et al. (2022). Increased aerosol concentrations in the high Arctic attributable to changing atmospheric transport patterns. *npj Climate and Atmospheric Science*, *5*(1), 62. https://doi.org/10.1038/s41612-022-00286-y

Pokrovsky, O. S., Karlsson, J., & Giesler, R. (2018). Freeze-thaw cycles of Arctic thaw ponds remove colloidal metals and generate low-molecular-weight organic matter. *Biogeochemistry*, *137*(3), 321–336. https://doi.org/10.1007/s10533-018-0421-6

Rantanen, M., Karpechko, A. Y., Lipponen, A., Nordling, K., Hyvärinen, O., Ruosteenoja, K., et al. (2022). The Arctic has warmed nearly four times faster than the globe since 1979. *Communications Earth & Environment*, *3*(1), 168. https://doi.org/10.1038/s43247-022-00498-3

Rijkenberg, M. J., Slagter, H. A., Rutgers van der Loeff, M., van Ooijen, J., & Gerringa, L. J. (2018). Dissolved Fe in the deep and upper Arctic Ocean with a focus on Fe limitation in the Nansen Basin. *Frontiers in Marine Science*, *5*, 88. https://doi.org/10.3389/fmars.2018.00088

Rudnick, R. L., & Gao, S. (2003). Composition of the continental crust. In H. D. Holland & K. K. Turekian (Eds.), *Treatise on Geochemistry* (pp. 1–64). Pergamon. https://doi.org/10.1016/B0-08-043751-6/03016-4

Schlesinger, W. H., Klein, E. M., & Vengosh, A. (2017). Global biogeochemical cycle of vanadium. *Proceedings of the National Academy of Sciences*, *114*(52), E11092–E11100. https://doi.org/10.1073/pnas.1715500114

Schmale, J., Zieger, P., & Ekman, A. M. (2021). Aerosols in current and future Arctic climate. *Nature Climate Change*, *11*(2), 95–105. https://doi.org/10.1038/s41558-020-00969-5

Sebaaly, A. P., van Rijn, F., Hanna, K., & Boily, J. F. (2025). Ice as a kinetic and mechanistic driver of oxalate-promoted iron oxyhydroxide dissolution. *Proceedings of the National Academy of Sciences of the United States of America*, *122*(35), e2507588122. https://doi.org/10.1073/pnas.2507588122

Shaw, G. E. (1995). The Arctic haze phenomenon. *Bulletin of the American Meteorological Society*, *76*(12), 2403–2413. https://doi.org/10.1175/1520-0477(1995)076<2403:tahp>2.0.co;2

Shelley, R. U., Morton, P. L., & Landing, W. M. (2015). Elemental ratios and enrichment factors in aerosols from the US-GEOTRACES North Atlantic transects. *Deep-Sea Research Part II*, *116*, 262–272. https://doi.org/10.1016/j.dsr2.2014.12.005

Shelley, R. U., Roca-Martí, M., Castrillejo, M., Sanial, V., Masqué, P., Landing, W. M., et al. (2017). Quantification of trace element atmospheric deposition fluxes to the Atlantic Ocean (>40 N; GEOVIDE, GEOTRACES GA01) during spring 2014. *Deep-Sea Research, Part A: Oceanographic Research Papers I*, *119*, 34–49. https://doi.org/10.1016/j.dsr.2016.11.010

Shen, H., Xue, L., Fan, G., Xu, H., Zhang, Z., Pan, G., et al. (2024). Trace metals reveal significant contribution of coal combustion to winter haze pollution in Northern China. *ACS ES&T Air*, *1*(7), 714–724. https://doi.org/10.1021/acsestair.4c00050

Stephens, M. P., Marsay, C. M., Schneebeli, M., Landing, W. M., Buck, C. S., & Geibert, W. (2024). Aerosol deposition and snow accumulation processes from beryllium-7 measurements in the central Arctic Ocean: Results from the MOSAiC expedition. *Journal of Geophysical Research: Oceans*, *129*(2), e2023JC020044. https://doi.org/10.1029/2023JC020044

Thomas, A. E., Bauer, P. S., Dam, M., Perraud, V., Wingen, L. M., & Smith, J. N. (2024). Automotive braking is a source of highly charged aerosol particles. *Proceedings of the National Academy of Sciences of the United States of America*, *121*(13), e2313897121. https://doi.org/10.1073/pnas.2313897121

Tovar-Sánchez, A., Duarte, C. M., Alonso, J. C., Lacorte, S., Tauler, R., & Galbán-Malagón, C. (2010). Impacts of metals and nutrients released from melting multiyear Arctic sea ice. *Journal of Geophysical Research*, *115*, C07003. https://doi.org/10.1029/2009JC005685

Wei, T., Dong, Z., Li, F., Kang, S., & Qin, X. (2025). Quantifying the distribution and origins of aerosol zinc across the Northern Hemisphere using stable zinc isotopes: A review. *The Journal of Hazardous Materials*, *491*, 137828. https://doi.org/10.1016/j.jhazmat.2025.137828

Weis, J., Chase, Z., Schallenberg, C., Strutton, P. G., Bowie, A. R., & Fiddes, S. L. (2024). One-third of Southern Ocean productivity is supported by dust deposition. *Nature*, *629*(8012), 603–608. https://doi.org/10.1038/s41586-024-07366-4

Whitmore, L. M., Jensen, L., Granger, J., Xiang, Y., Kipp, L., Pasqualini, A., et al. (2025). Multi-elemental tracers in the Amerasian Basin reveal interlinked biogeochemical and physical processes in the Arctic Ocean upper halocline. *Global Biogeochemical Cycles*, *39*(4), e2024GB008342. https://doi.org/10.1029/2024GB008342

Willis, M. D., Leaitch, W. R., & Abbatt, J. P. (2018). Processes controlling the composition and abundance of Arctic aerosol. *Reviews of Geophysics*, *56*(4), 621–671. https://doi.org/10.1029/2018RG000602

Xie, Z., Sun, L., Blum, J. D., Huang, Y., & He, W. (2006). Summertime aerosol chemical components in the marine boundary layer of the Arctic Ocean. *Journal of Geophysical Research*, *111*, D10309. https://doi.org/10.1029/2005JD006253

Yu, G., Zhang, Y., Yang, F., He, B., Zhang, C., Zou, Z., et al. (2021). Dynamic Ni/V ratio in the ship-emitted particles driven by multiphase fuel oil regulations in coastal China. *Environmental Science & Technology*, *55*(22), 15031–15039. https://doi.org/10.1021/acs.est.1c02612

Zhan, J., Gao, Y., Li, W., Chen, L., Lin, H., & Lin, Q. (2014). Effects of ship emissions on summertime aerosols at Ny–Alesund in the Arctic. *Atmospheric Pollution Research*, *5*(3), 500–510. https://doi.org/10.5094/APR.2014.059

Zhan, J., Li, W., Chen, L., Lin, Q., & Gao, Y. (2017). Anthropogenic influences on aerosols at Ny-Ålesund in the summer Arctic. *Atmospheric Pollution Research*, *8*(2), 383–393. https://doi.org/10.1016/j.apr.2016.10.010

Zhang, R., Jensen, L., Fitzsimmons, J., Sherrell, R., & John, S. (2019). Dissolved cadmium and cadmium stable isotopes in the western Arctic Ocean. *Geochimica et Cosmochimica Acta*, *258*, 258–273. https://doi.org/10.1016/j.gca.2019.05.028

Zhang, R., Jensen, L., Fitzsimmons, J., Sherrell, R. M., Lam, P., Xiang, Y., & John, S. (2021). Iron isotope biogeochemical cycling in the Western Arctic Ocean. *Global Biogeochemical Cycles*, *35*(11), e2021GB006977. https://doi.org/10.1029/2021GB006977

Zhao, J., Zhang, Y., Xu, H., Tao, S., Wang, R., Yu, Q., et al. (2021). Trace elements from ocean-going vessels in East Asia: Vanadium and nickel emissions and their impacts on air quality. *Journal of Geophysical Research: Atmospheres*, *126*(8), e2020JD033984. https://doi.org/10.1029/2020JD033984

Zhao, S., Yan, J., Lin, Q., Yao, L., Park, K., Jung, J., et al. (2022). Changes in aerosol particle composition during sea fog formation events in the sea ice regions of the Arctic Ocean. *Atmospheric Environment*, *272*, 118943. https://doi.org/10.1016/j.atmosenv.2022.118943

Zheng, L., Minami, T., Konagaya, W., Chan, C., Tsujisaka, M., Takano, S., et al. (2019). Distinct basin-scale-distributions of aluminum, manganese, cobalt, and lead in the North Pacific Ocean. *Geochimica et Cosmochimica Acta*, *254*, 102–121. https://doi.org/10.1016/j.gca.2019.03.038